

Dark-State-Mediated Efficient Energy Trapping in a Model GFP Chromophore

Elisabeth Gruber,[†] Lars H. Andersen,^{*,†} Laurence H. Stanley,[‡] Jan R. R. Verlet,^{*,‡} Ivan S. Avdonin,[¶] and Anastasia V. Bochenkova^{*,¶}

[†]*Department of Physics and Astronomy, Aarhus University, 8000 Aarhus C, Denmark*

[‡]*Department of Chemistry, Durham University, Durham DH1 3LE, United Kingdom*

[¶]*Department of Chemistry, Lomonosov Moscow State University, Moscow 119991, Russia*

E-mail: lha@phys.au.dk; j.r.r.verlet@durham.ac.uk; bochenkova@phys.chem.msu.ru

Abstract

The functional properties of photoactive proteins are governed by the interplay between bright and dark excited states. While the bright states are well-studied, the dark states, which are fundamental to photostability and light harvesting, are notoriously difficult to characterize. Here, we report the direct observation and full characterization of an optically dark, low-lying singlet excited state in the isolated anion of the *meta* green fluorescent protein (GFP) chromophore. Using a combination of ultrafast time-resolved action-absorption and photoelectron spectroscopy, we have captured the formation of this state in 100 fs and measured its remarkably long lifetime of 94 ps. We unambiguously assign its charge-transfer character and reveal the precise trapping mechanism through high-level *ab initio* calculations. Our findings uncover a photoprotective mechanism in biomolecular anions where ultrafast internal conversion quenches electron emission, stabilizing long-lived electronic excitation even when the energy exceeds the electron detachment threshold.

Introduction

At first sight, one might think that optically dark states (*i.e.* electronic states having a small dipole coupling with the electronic ground state, or dark because of symmetry reasons) are of little interest. They do, however, play an important role in the photophysics of chromophores as they may be populated through conical intersections after photoexcitation to higher lying bright electronic states. Upon internal conversion, they may thus act as ‘trapping states’ with long lifetimes and little fluorescence. In photosynthetic complexes, symmetry-forbidden dark states are relevant in light-harvesting and for photoprotection by carotenoids.^{1–3} When excited to the bright S_2 state, the carotenoid chromophore relaxes within 50-300 fs to the optically inactive S_1 state, which is then involved in the pigment-pigment energy transfer process. In carotenoids containing carbonyls, it is found that the lifetime of the dark charge-transfer states is strongly solvent dependent.⁴

Chromophores featuring long-lived dark excited states are of considerable interest for their potential in advanced technologies. They might be applicable in biomimetic electronic and memory devices, where there is a need to switch between light emitting and non-emitting states.⁵ The utility of these states also extends to sensing and photoprotection. Their long lifetime may enable their use as ”dark donors“ in Förster resonance energy transfer, providing a background-free signal for biosensing.⁶ Simultaneously, their capacity to absorb harmful high-energy photons via a higher-lying bright state and to dissipate the energy as heat from a stable dark state makes them highly efficient energy sinks, offering a strategy for enhancing the durability of polymers and synthetic materials.⁷ Given the above, it is not surprising that there has been a desire to develop photo-active proteins with engineered dark states. Specifically, dark charge-transfer states have been studied in the chromophores of the photoactive yellow protein (PYP)⁸ and the Green Fluorescent Protein (GFP)^{9–11} through their meta-derivatives.

Solvation can strongly influence dark states, underscoring the need to understand their intrinsic spectroscopy and dynamics. Gas-phase spectroscopy uniquely enables such stud-

ies by isolating the intrinsic properties. Yet, the optically forbidden nature of dark states renders their investigation experimentally challenging, especially in the gas phase where ion densities are low. To overcome this problem we apply action-absorption spectroscopy, developed for studies of chromophore ions at ion-storage rings both in terms of spectroscopy^{12,13} and lifetimes,^{14,15} alongside photoelectron spectroscopy^{16,17} and high-level quantum chemical calculations.^{18–20}

Here we focus on the chromophore of the GFP. This protein, with 238 amino acids, has a rigid 11-stranded β -barrel structure with a 4-(p-hydroxybenzylidene)-5-imidazolinone (pHBI) chromophore at the centre, well protected from external solvents. The protein is widely used for imaging purposes in biological samples due to its fluorescent properties.²¹ Numerous studies of GFP-model chromophores have been conducted over the past almost twenty years. In particular, a dimethyl derivative of pHBI, called para-HBDI is used as a model for the chromophore of the protein. For this molecule, the absorption spectrum within the visible range is dominated by the intense $S_0 \rightarrow S_1$ transition at ~ 480 nm¹² (see Fig. 1), with a band origin, determined by cryogenic spectroscopy, at 481.5 nm.²² Above the electron-detachment threshold, electron emission proceeds through autodetachment of vibrational resonances (VRs), whereas below the threshold there may appear a significant contribution from sequential multiphoton absorption in action-absorption spectra mediated by the strong $S_0 \rightarrow S_1$ transition in para-HBDI.^{11,12,19,23} The separation between one and multiphoton contributions is conveniently done by the use of fast fs-laser pulses.²⁴

Moving the oxygen atom on the phenolate ring from the *para* to the *meta* position (see Fig. 1) significantly alters the low-energy part of the HBDI photoabsorption spectrum, which is relevant to its photochemistry.¹¹ The absence of valence resonance structures of the meta-HBDI anion in the electronic ground state causes an effective decoupling of the isoelectronic π -systems of the phenolate and imidazolinone rings. Calculations of the relevant π and π^* orbitals reveal that the $S_0 \rightarrow S_1$ transition has a significant charge-transfer character, implying that this S_1 state is strongly influenced by the solvation of a polar solvent (*e.g.* water). It

is predicted to lie at the far red edge of the visible spectrum (~ 700 nm) with a very low oscillator strength.¹¹

This work offers direct spectroscopic access to the dark S_1 state of meta-HBDI, revealing its lifetime and energy. The photoresponse of the anion has been studied in the spectral region from 350 to 700 nm in the gas phase. The presence of an optically dark, low-lying excited state, which has been predicted theoretically, is confirmed through action-absorption and photoelectron spectroscopy. The charge-transfer character of the $S_0 \rightarrow S_1$ transition is affirmed by measuring a significant blue shift when the chromophore is complexed with betaine, a molecule with a dipole moment of almost 12 D. Excited-state dynamics is studied using both pump-probe action and photoelectron spectroscopies and is supported by *ab initio* calculations to provide a comprehensive understanding of the energy flow. We find a sub-nanosecond excited-state lifetime for the dark S_1 state, whereas the bright S_2 state decays to S_1 on an ultrafast timescale of 100 fs. We show that internal conversion between S_2 and S_1 through a conical intersection dominates over electron detachment when the anion is excited at 400 nm, despite being well above its photodetachment threshold (~ 490 nm). This results in efficient trapping of electronic excitation in the dark excited state located in the near-IR region. Our results offer a new and exquisite window into the sensitivity and role of dark states in fluorescent proteins.

Results and discussion

Nature and Energy Landscape of Excited States

Figure 1 shows the absorption spectrum of meta-HBDI in the spectral region from 350 to 700 nm, covering transitions from the electronic ground state S_0 into the first excited state S_1 (weak absorption between 550 nm and 700 nm) and into the second excited state S_2 (below 400 nm). The vertical electron detachment energy (VDE) for meta-HBDI was previously determined to be in the range of 2.40 – 2.54 eV \pm 0.1 eV.¹¹ The significant spread was

due to inhomogeneous broadening caused by internal rotation about the single C-C bridge bond in the electronic ground state. Indeed, MP2/(aug)-cc-pVTZ calculations reveal two rotamers in meta-HBDI, separated by an energy of 0.05 eV with an interconversion barrier of 0.46 eV (see Fig. S1). While these rotamers are spectroscopically indistinguishable at their equilibrium planar geometries, rotation along the interconversion coordinate lowers the VDE, with a maximum reduction of 0.2 eV at the transition state. Here, using photoelectron spectroscopy, we refine the experimental VDE and also find the adiabatic detachment energy to be 2.63 and 2.30 ± 0.05 eV, respectively.

The broad and intense absorption observed between 400 and 500 nm – near and above the electron-detachment threshold – arises from two main processes: direct electron detachment, and excitation of vibrational resonances associated with a non-valence, electronically dipole-bound state.¹¹ States with little vibrational excitation are truly bound and are observed experimentally through sequential two-photon absorption. In contrast, excess vibrational energy in the radical core can promote these states into the continuum, where they manifest as autodetaching resonances.^{17,25,26} In meta-HBDI, direct transitions from S_0 to these states are spectrally distinct from transitions to the valence excited states: S_1 in the near-IR, which is electronically bound, and S_2 in the UV, which is embedded in the continuum and is therefore metastable against electron emission.

The charge-transfer nature of the $S_0 \rightarrow S_1$ transition was revealed by zwitterion tag action spectroscopy (ZITA spectroscopy).²⁷ The excitation of a charge-transfer (CT) transition significantly redistributes electron density within the chromophore. This redistribution alters the Coulombic interaction with any nearby dipole, making CT transitions exceptionally sensitive to their electrostatic environment, including solvent interactions. The different

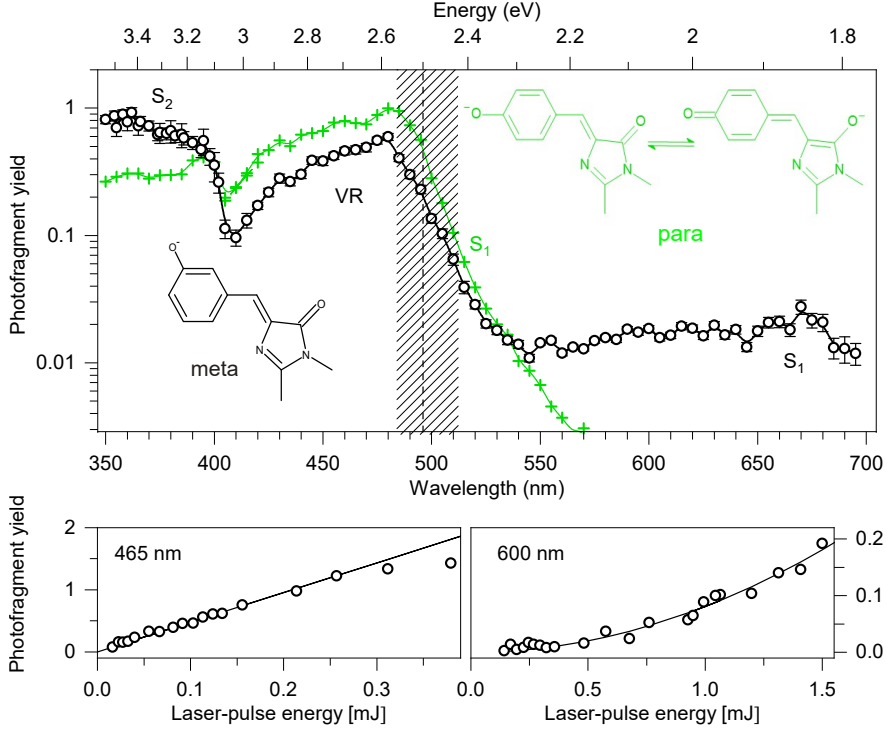


Figure 1: Action-absorption spectrum of meta-HBDI (black data points) in comparison to para-HBDI (green data points). Notice the logarithmic vertical axis. The vertical line shows the electron-detachment threshold for the meta chromophore. Between 350 and 500 nm prompt action is detected after single-photon absorption (photofragment yield increases linearly with the laser-pulse energy, presented here for 465 nm in the lower graph) and associated with excitation into S₂ and vibrationally resonant (VR) photodetachment out of the dipole-bound state. The weak absorption between 550 and 700 nm for meta-HBDI is attributed to excitation of the dark S₁ state. Sequential absorption of two photons is necessary to cause fragmentation (photofragment yield increases quadratically with the laser-pulse energy, presented here for 600 nm in the lower graph). Data in the region 550 and 700 nm is normalized according to the quadratic laser-power dependence.

interaction strength between the ion and the dipole in the ground and excited states leads to a blueshift of the absorption band. Thereby, the extent of the shift is a measure of the CT degree. With a 11.9 D dipole moment arising from its quaternary ammonium and carboxylate termini,²⁸ the zwitterion betaine is an excellent probe molecule for ZITA spectroscopy.^{27,29,30}

The absorption of the betaine-meta-HBDI complex shows a rather different picture with a more than 100 nm blue-shift for the S₀ → S₁ transition energy, pointing to a strong CT character (see Fig. 2). Indeed, the calculated π and π^* orbitals, which are primarily involved in the excitation, show that the S₀ → S₁ transition is associated with a significant electron-

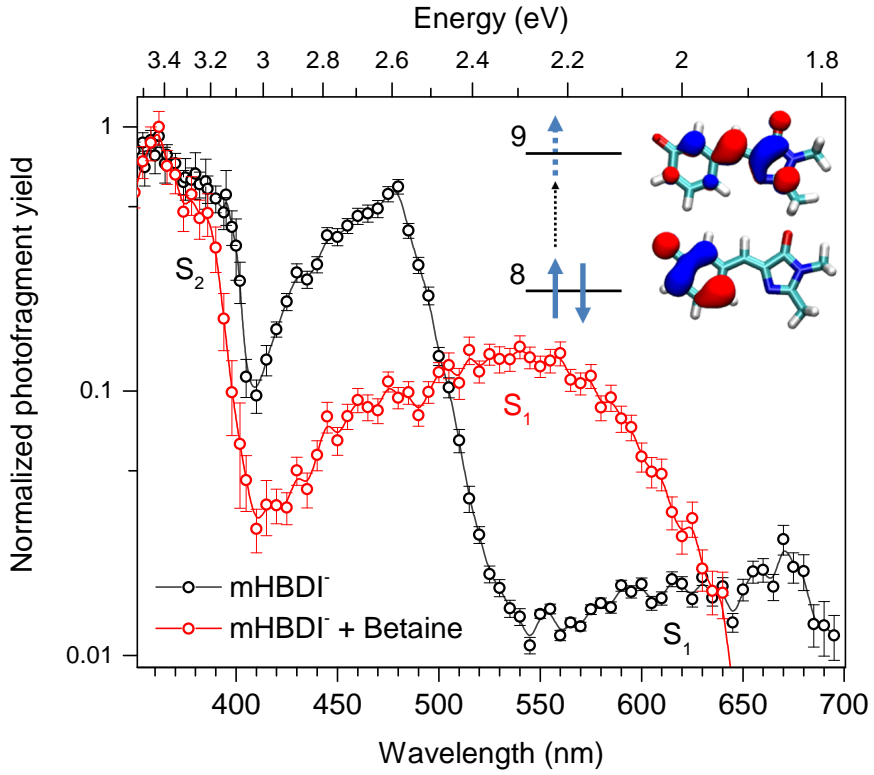


Figure 2: Prompt action spectrum of meta-HBDI (black data points) in comparison with meta-HBDI complexed with betaine (red data points). A strong blueshift of the S_0 - S_1 transition energy in the meta-HBDI - betaine complex reflects a strong CT character. Calculations of the π and π^* orbitals, which are primarily involved in the excitation, show that the transition is connected to charge transfer from the phenolate ring into the imidazolinone ring. Only little blueshift for the transition into S_2 is observed.

density transfer from the phenolate ring to the imidazolinone ring (see inset in Fig. 2). Only a small blueshift is observed for the 400 nm transition into S_2 , pointing to a much lower CT character.

The presence of the low-lying dark state in the meta-HBDI anion is further supported by photoelectron spectroscopy and high-level *ab initio* calculations. Figure 3 shows the two-dimensional photoelectron spectrum^{17,31,32} of meta-HBDI recorded with nanosecond laser pulses with one-dimensional cuts at specific photon energies. Several distinct regions, labeled (i) – (v), are highlighted for discussion. With reference to the energy levels, calculated using

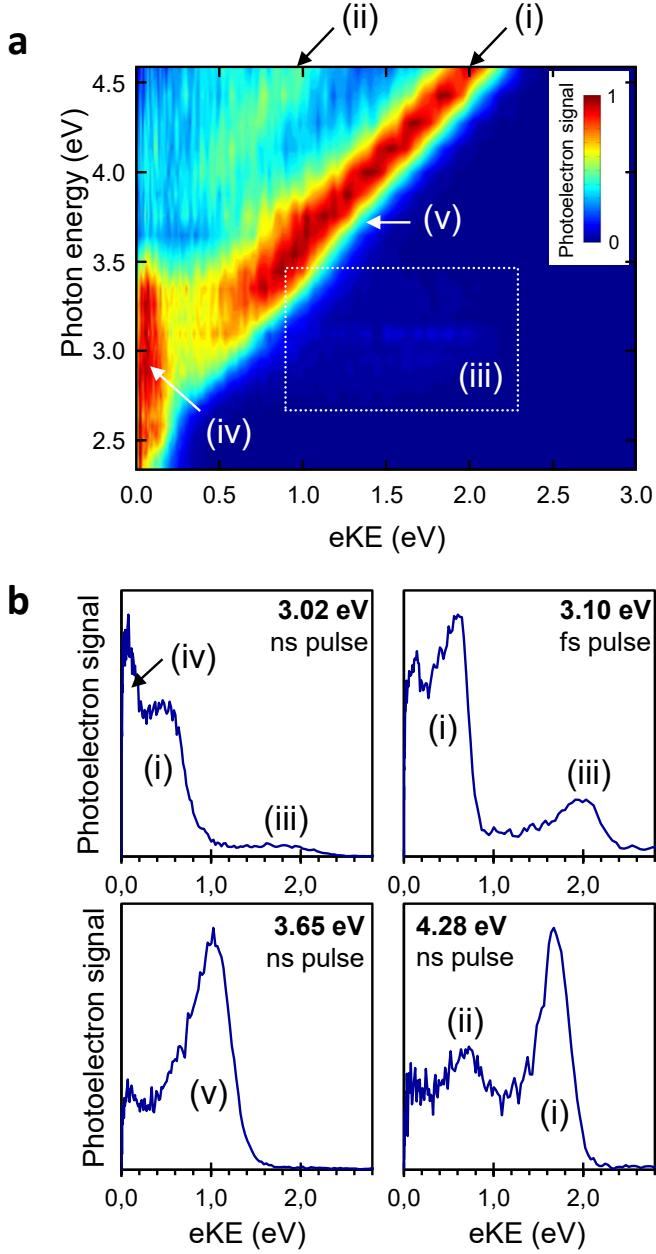


Figure 3: Photoelectron spectra of the meta-HBDI anion. (a) Two-dimensional photoelectron spectrum recorded with nanosecond laser pulses. (b) One-dimensional spectral cuts at specified excitation energies. For comparison, the spectrum at 3.10 eV was acquired with femtosecond pulses, contrasting with the 3.02 eV spectrum measured using ns pulses.

multiconfiguration quasi-degenerate perturbation theory XMCQDPT2³³ (see Fig. 4 and the SI for computational details), these regions correspond to the following processes:

- i) The linear relation between the photon energy and the energy of the outgoing electron

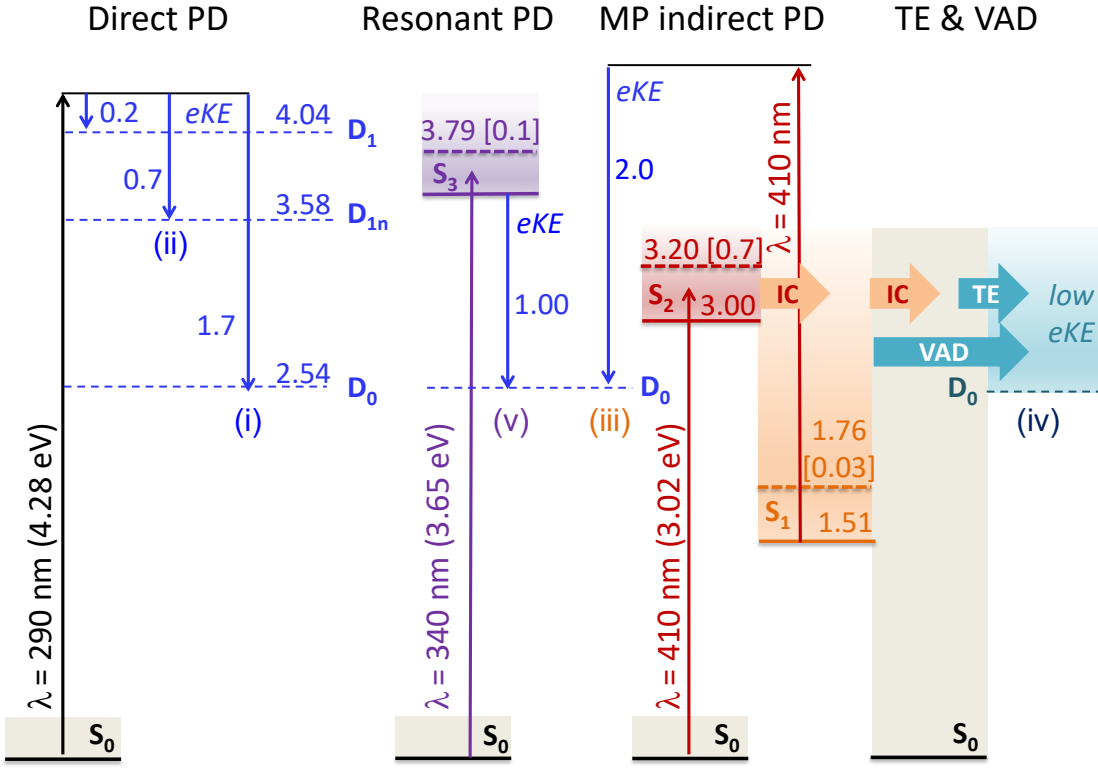


Figure 4: Wavelength-dependent photodetachment (PD) mechanisms for the meta-HBDI anion. The energy-level diagram, calculated at the XMCQDPT2/SA(3)-CASSCF(16,14)/(aug)-cc-pVDZ level, shows pathways for different excitation energies: direct PD; resonant PD through the S_3 shape resonance; multiphoton (MP) indirect PD via the S_1 state after internal conversion (IC) from the S_2 Feshbach resonance; thermionic emission (TE) from S_0 ; and vibrational autodetachment (VAD) from S_1 . Channels (i) – (v) are identified in the experimental 2D photoelectron spectrum (Fig. 3). Energies (in eV) and oscillator strengths (in brackets) are provided for key transitions. Adiabatic and vertical energies are shown as solid and dashed lines, respectively, with colored areas representing the vibrational manifold. Blue arrows indicate the electron-detachment process, labeled with the resulting electron kinetic energy (eKE).

corresponds to direct photodetachment $h\nu + S_0 \rightarrow D_0 + e^-$. Excitation at 4.28 eV yields the most unperturbed photoelectron spectrum (see Fig. 3b, lower right panel). We determine adiabatic and vertical electron detachment energies of 2.30 ± 0.05 eV and 2.63 ± 0.05 eV, respectively, which are consistent with and refine the previously measured values of $2.40 - 2.54 \pm 0.1$ eV.¹¹ The calculated vertical detachment energy (D_0) is 2.54 eV, which corresponds well to the ridge of (i) in the photoelectron spectrum.

- ii) Similarly, region (*ii*) corresponds to direct detachment to an excited state in the neutral radical D_{1n} . The calculated difference between D_{1n} and D_0 is 1.04 eV, which matches the experimental gap.
- iii) The appearance of region (*iii*) with an electron-kinetic energy higher than that of direct one-photon detachment provides evidence for a two-photon detachment process. This mechanism requires the first photon to populate an intermediate state of the anion, from which a second photon, absorbed within the same laser pulse, causes electron detachment. In the ns-laser experiments, the weak signal in region (*iii*) is assigned to photodetachment from the intermediate S_1 state. Electrons ejected from this state are born with an adiabatic excitation energy (AEE) of 1.51 eV (see Fig. 4). For a process where S_1 is populated by internal conversion from S_2 , the sequential absorption of two 3.02 eV photons yields photoelectrons with a maximum kinetic energy of $AEE(S_1) + h\nu - VDE(D_0) \sim 2.0$ eV (Fig. 3b, upper left panel). The peak is significantly enhanced with 400 nm (3.1 eV) fs-laser pulses (Fig. 3b, upper right panel) due to the higher probability of absorbing a second photon from the intermediate S_1 state within the tens-of-fs pulse duration compared to the much longer 5 ns pulse. Although absorption from S_2 could yield a peak at $AEE(S_2) + h\nu - VDE(D_1) \sim 2.0$ eV, its lifetime is much shorter (see below) than that of S_1 and comparable to the femtosecond pulse duration, rendering this pathway less probable.
- iv) The region of low-energy electrons (*iv*) is due to internal conversion from S_2 to S_1 and further to S_0 followed by statistical thermionic emission from the ground state³⁴ or vibrational autodetachment out of the electronically bound S_1 state.²² This channel may also contain a contribution from sequential absorption of multiple photons from the ns-laser pulses (duration \sim 5 ns). Internal conversion is here faster than autodetachment out of S_2 . This resonance state is of a Feshbach type with respect to the open D_0 continuum,¹¹ and hence electronic autodetachment out of this state is a two-

electron process, which becomes slower than the sub-ps nuclear photoresponse in this region.^{35,36}

- v) Finally, in region (v) between the 3.6 eV and 3.9 eV photon energy there is a slight broadening in the signal, which may be caused by the opening of the resonant channel $h\nu + S_0 \rightarrow S_3 \rightarrow D_0 + e^-$ (Figs. 3a and 3b, lower left panel). The calculated position of S_3 supports this assignment (see Fig. 4). This state is a shape resonance with respect to the D_0 continuum,¹¹ and one-electron autodetachment dominates the signal in region (v).^{20,37}

We have shown that action-absorption spectroscopy has direct spectroscopic access to the near-IR dark S_1 state of charge-transfer character. The presence of this electronically bound state is also confirmed by photoelectron spectroscopy. It is observed through a multi-photon indirect photodetachment process: initial excitation populates the bright S_2 state above the detachment threshold, followed by internal conversion to the S_1 state and subsequent electron detachment via absorption of a second photon. From the presence of the low-eKE part in the two-dimensional photoelectron spectrum, it also follows that internal conversion from S_2 competes with electron autodetachment out of this resonance state. In the following, we present direct measurements of the S_2 and S_1 lifetimes using femtosecond pump–probe spectroscopy that integrates time-resolved action-absorption and photoelectron detection.

Dynamics of Excited States

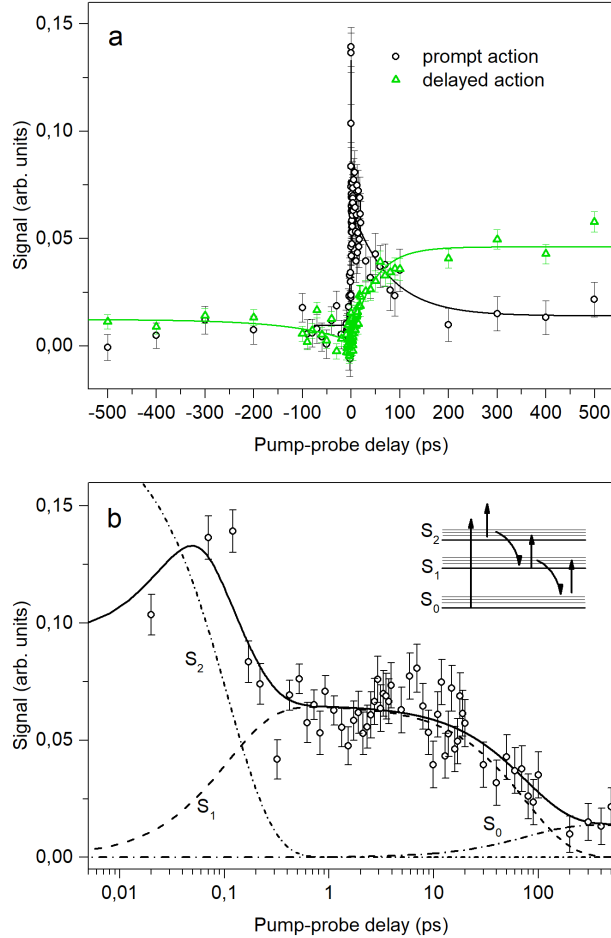


Figure 5: Excited-state lifetime measured in pump-probe experiments at the ion storage ring SAPHIRA. The molecules were first excited into S_2 by a 400 nm pump pulse and then probed by a 800 nm probe pulse. The experimental setup enables the detection of prompt (within the first 10 μ s after photoexcitation) as well as delayed (after 10 μ s up to several ms after photoexcitation) photofragmentation. The upper graph (a) shows the prompt and delayed fragmentation as a function of the pump-probe delay on a linear timescale. While the lifetime of S_2 and S_1 can be probed by detecting prompt fragmentation, the delayed action shows the ground state recovery. In the lower graph (b), the signal of the prompt action is plotted on a logarithmic time scale and shows that the decay consists of a fast and a slow component. The fast decay of $100 \text{ fs} \pm 26 \text{ fs}$ corresponds to the fast relaxation out of S_2 with subsequent trapping in S_1 for $94 \text{ ps} \pm 11 \text{ ps}$. The solid line represents a fit through the data points using a rate model indicated by the inserted schematic. The dashed lines show the calculated population of S_2 , S_1 and S_0 .

The femtosecond pump-probe technique combined with time-resolved action-absorption spectroscopy enables simultaneous monitoring of both excited-state decay and ground-state recovery. Figure 5 shows the measured prompt and delayed photo-induced yields of neutrals. The fast ~ 100 fs decay of the prompt signal is attributed to ultrafast internal conversion from S_2 to S_1 . The slower 94 ps decay, appearing as the long-lived decaying component of the prompt response, is attributed to the decay out of S_1 . It corresponds to the repopulation of the S_0 ground state, fully consistent with the recovery dynamics revealed in the delayed action.

The time-resolved photoelectron spectrum is plotted in Fig. 6. It is evident that also here a very fast as well as a long-lived component exist. The fast component, which has a kinetic energy extending to ~ 1.7 eV also decays within the first 100 fs. The spectrum of this feature

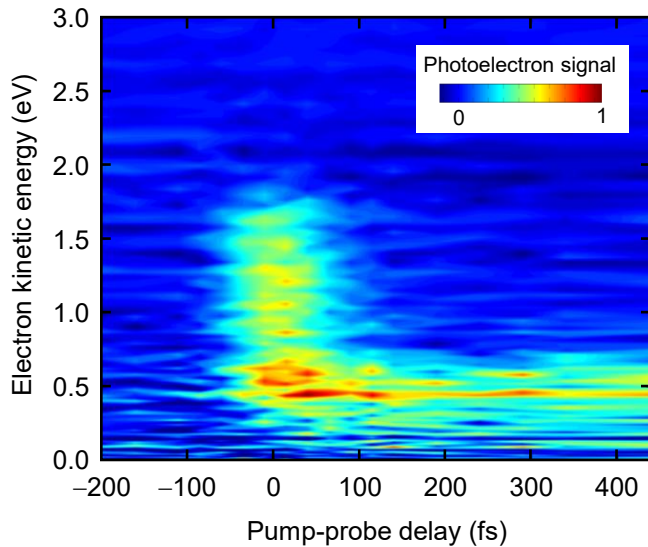


Figure 6: Photoelectron yield in pump-probe measurements (400 nm + 800 nm). The signal between 0.5 and 1.5 eV decays rapidly and is linked to the relaxation out of the S_2 state. The signal at 0.4 eV remains for a longer time due to population trapping in the dark S_1 state from the S_2 state. The ground-state recovery is not detected due to insufficient photon energy in the 800 nm probe pulse.

is consistent with detachment from the S_2 state. The S_2 -signal decay is commensurate with the appearance of a new spectral feature with a kinetic energy peaking around 0.45 eV, corresponding to a binding energy of about 1.1 eV. This can be assigned to the S_1 -excited state, which lies about 1.2 eV lower than the S_2 state, according to Fig. 1. As soon as the electronic ground state is reached, the absorption of a 1.55 eV (800 nm) probe photon does not suffice to lead to electron detachment. The S_2 excited-state signal is observed to decay with a lifetime of \sim 90 fs, which is in excellent agreement with the measurement by the action-absorption spectroscopy technique.

Trapping Mechanism

The experimental results are rationalized by the aid of *ab initio* calculations. We find that the S_1 state of the meta-HBDI anion is optically dark in the Franck-Condon region, whereas the $S_0 \rightarrow S_2$ transition is bright (see Fig. 4). The calculated vertical excitation energy of the $S_0 \rightarrow S_1$ transition is 1.76 eV (704 nm) with an oscillator strength of 0.03. The red-shifted value and the very low intensity of the first excitation are attributed to its nature connected to the transfer of charge and electron density from phenolate to the imidazolinone ring (see Figs. S2-S3). The second transition is the brightest in the absorption spectrum, with a calculated vertical excitation energy of 3.2 eV (387 nm) and an oscillator strength of 0.7. It involves a local redistribution of electron density within the π -system of the imidazolinone ring (Figs. S2-S3).

In the present study, ZITA action-absorption spectroscopy of the meta-HBDI anion complexed with betaine directly confirms the high charge-transfer character of the S_1 state and the low charge-transfer character of the S_2 state. The energetics of the S_1 state is also confirmed experimentally. In action-absorption spectroscopy, a broad absorption profile between 550–700 nm is assigned to direct excitation of S_1 . The broad Franck-Condon envelope of this band is characteristic of a charge-transfer transition. Furthermore, photoelectron spectroscopy gives a vertical electron binding energy of 1.1 eV for the S_1 state. When combined

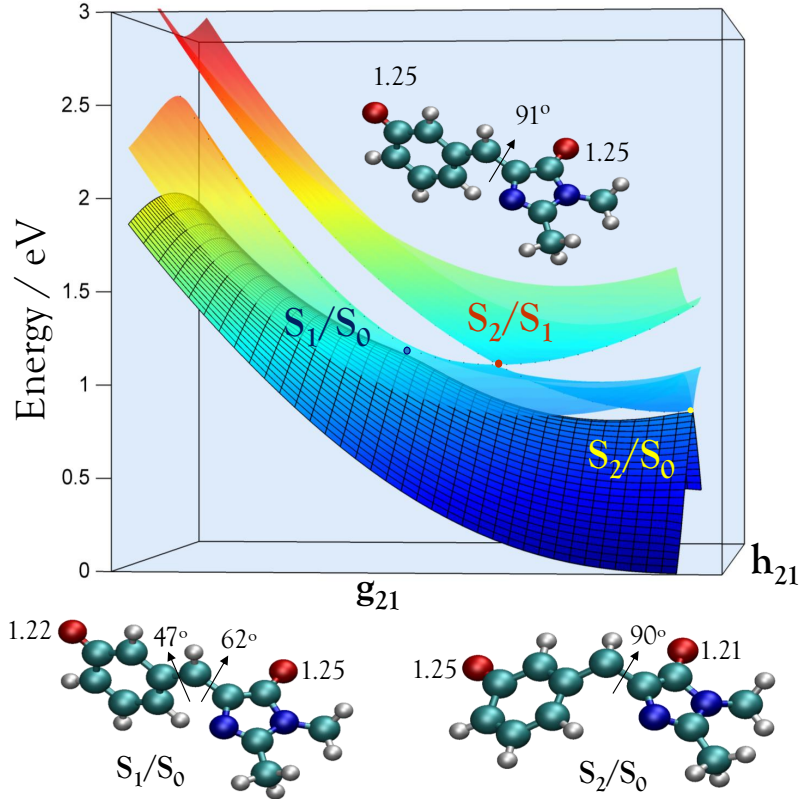


Figure 7: CASSCF(16,14)/(aug)-cc-pVDZ potential-energy surface illustrating the conical intersections governing the excited-state dynamics of the meta-HBDI anion. The surface is plotted in the branching plane of the S_2/S_1 conical intersection, spanned by the gradient difference vector (\mathbf{g}_{21}) and the nonadiabatic coupling vector (\mathbf{h}_{21}). Also shown are the minimum-energy conical intersection structures, with key torsional angles in the bridge moiety and O–C bond lengths (in Å) indicated. This representation highlights how nuclear motion along these directions defines the nonradiative decay along two competing branches involving three conical intersections. Note that the intermediate S_1 state traps the excited-state population at the planar equilibrium geometry. The S_1/S_0 minimum-energy conical intersection on the dark branch is the lowest-energy pathway for internal conversion to the ground state (see Fig. 8).

with the measured VDE(D_0) of 2.6 eV, this yields an $S_0 \rightarrow S_1$ adiabatic excitation energy of 1.5 eV, a value in excellent agreement with the calculated result of 1.51 eV.

Analysis of electron density and charge distribution in S_2 and S_1 reveals that excitation dramatically reduces the π -bond order of a key C=C bridge bond – by 2.2 in S_2 and 1.6 in S_1 – which equalizes the bridge bonds and facilitates ultrafast internal conversion via

bond rotation. Furthermore, excited-state resonance couples the valence structures of S_2 and S_1 , scrambling their isoelectronic π -subsystems and equalizing charge localization probability between the phenolate oxygen and the bridge carbon, thereby altering the effective π -system partition (see Fig. S4). Rotation around the bridge C=C bond serves as the key reaction coordinate, driving the system toward the S_2/S_1 conical intersection by equalizing charge localization probability between the states. This leads to the highly efficient internal conversion observed between the S_2 and S_1 states.

Three conical intersections (CI) are located that interconnect the S_2 , S_1 , and S_0 states, which are relevant to the relaxation dynamics of the meta-chromophore in the gas phase. Fig. 7 shows the potential energy surfaces of S_2 , S_1 , and S_0 in the branching plane of the S_2/S_1 CI. The initial relaxation through the peaked S_2/S_1 CI occurs barrierless (Fig. S5) and is therefore very fast, in agreement with the experimental finding. The decay results in population of the S_1 state despite the open electron-detachment channel. However, a bifurcation at the S_2/S_1 CI funnels the S_1 population toward two distinct conical intersections with the ground state (Fig. 7). These two CIs are differentiated by the character of the first excited state: one acquires the CT character of the dark S_1 state, while the other retains the character of the bright S_2 state. Therefore, they are labeled as S_1/S_0 and S_2/S_0 , respectively.

The calculated energy-level diagram identifies the location of the minimum-energy conical intersections (MECIs) governing the non-adiabatic transitions between the S_2 , S_1 , and S_0 states (see Fig. 8). Following efficient internal conversion from S_2 , the meta-HBDI anion becomes trapped in the planar equilibrium geometry of the S_1 state. This trapping occurs because the S_2/S_0 and S_1/S_0 MECIs lie 0.55 eV and 0.41 eV higher in energy, respectively. The two decay pathways are structurally distinct: the S_2/S_0 CI involves rotation about the double C=C bridge bond, a pathway that could lead to isomerization. In contrast, the S_1/S_0 CI is characterized by twisting about both bridge bonds and significant pyramidalization of the bridge carbon (see Fig. 7 and Fig. S6). In the gas phase, the relaxation proceeds predominantly along this latter pathway, resulting in a long-lived non-fluorescent trapping

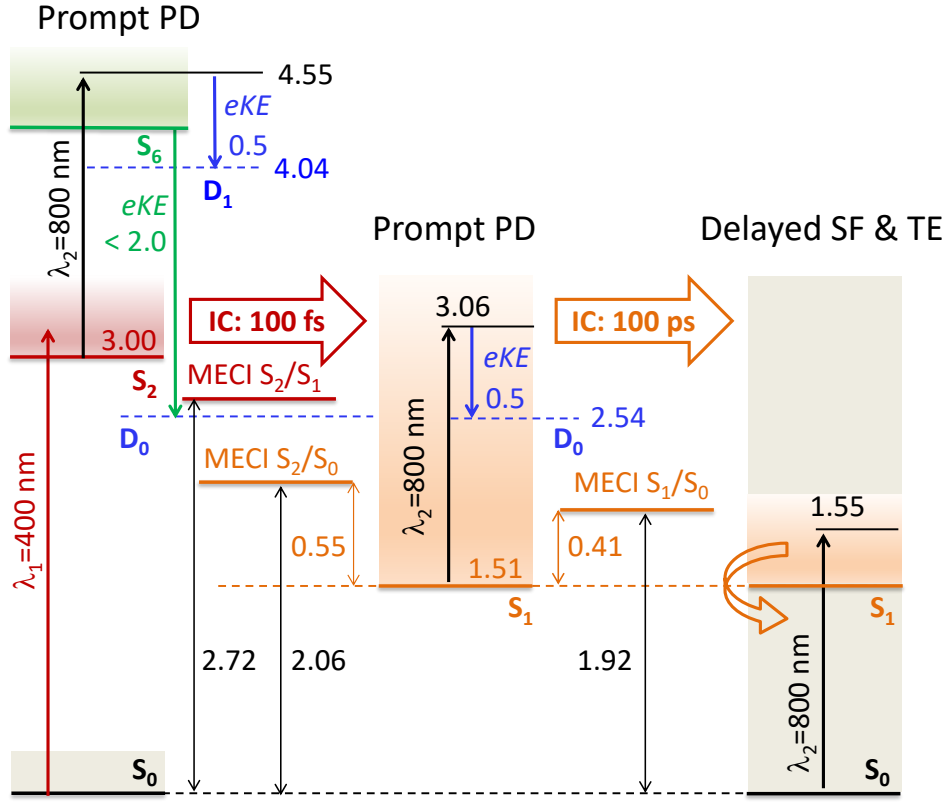


Figure 8: Trapping mechanism in the meta-HBDI anion. The XMCQDPT2/SA(3)-CASSCF(16,14)/(aug)-cc-pVDZ diagram shows relative energies of key electronic states and minimum-energy conical intersections (MECI) between the S_2 , S_1 , and S_0 states. Shown are also the prompt and delayed channels in pump (λ_1) – probe (λ_2) spectroscopy. The excited-state decay is registered both by measuring the energy of emitted electrons and by counting neutrals in prompt photodetachment (PD) channels. The ground-state recovery is measured as a delayed signal through counting neutrals following statistical fragmentation (SF) and thermionic emission (TE) from S_0 . Energies are in eV.

state that ultimately decays to the ground state without isomerization.

The photoinduced dynamics, studied using femtosecond pump–probe spectroscopy, is characterized by two complementary methods: (1) time-resolved action-absorption spectroscopy, which monitors prompt and delayed neutrals; and (2) photoelectron spectroscopy, which detects prompt electrons generated by direct photodetachment from the excited states. Direct detachment out of S_2 should comply with the Slater rules. In other words, two-electron processes are forbidden in the dipole approximation. Therefore, following 400 nm excitation of S_2 in meta-HBDI, an 800 nm probe photon can detach an electron from S_2 with the most

probable eKE of 0.5 eV (D_1), leaving the neutral with 0.1 eV of vibrational energy (Fig. 8). Alternatively, the probe photon can promote the anion from S_2 to a higher-lying resonance at \sim 4.6 eV, which autodecays, producing a broad electron kinetic energy distribution up to 2.0 eV across all open continua (D_1 , D_{1n} , and D_0). The experimental eKE distribution of up to \sim 1.7 eV observed at early times (Fig. 6) is consistent with both direct and resonant photodetachment pathways, which leave some vibrational energy in the neutral core. This is supported by the XMCQDPT2 calculations, which identify an excited state at 4.6 eV at the ground-state equilibrium geometry, with a non-negligible oscillator strength of 0.06 for the $S_2 \rightarrow S_6$ transition (see Fig. 8).

If internal conversion to S_1 occurs first, the same probe detaches an electron from S_1 , producing electrons with an energy of 0.5 eV (D_0) and a vibrationally hot neutral with 1.59 eV of excess energy. The significant narrowing of the eKE distribution peaking at 0.45 eV after 100 fs (Fig. 6) confirms the direct photodetachment pathway. Repopulation of the S_2 state from S_1 by the 800 nm probe is negligible due to the vanishing oscillator strength of this transition (Fig. 8). Following internal conversion to S_0 , the 800 nm excitation leads to repopulation of the electronically bound S_1 state, resulting in slow SF and TE from the hot ground state after internal conversion. The excited-state decay and ground-state recovery align well with the prompt and delayed signals observed in our pump-probe action-absorption experiments (Fig. 5).

The excited-state population is trapped in S_1 due to the presence of a barrier along the minimum-energy pathway that leads from the planar S_1 equilibrium structure to the highly twisted S_1/S_0 conical intersection. The XMCQDPT2/SA(3)-CASSCF(16,14)/(aug)-cc-pVDZ barrier of 0.41 eV is associated with reaching the lowest-lying S_1/S_0 CI with a sloped topography along the dark branch (see Fig. 8 and Fig. S6). Quasi-equilibrium theory for a microcanonical ensemble predicts a statistical lifetime of 98 ps for the S_1 excited state at 300 K after 400 nm excitation (Figs. S7-S8), a value that agrees perfectly with our experimental findings.

Conclusions

The spectroscopy and excited-state dynamics of meta-HBDI were studied by performing action spectroscopy and femtosecond pump-probe experiments. Our action-photoabsorption spectroscopy studies in vacuum directly revealed the presence of an optically dark S_1 state, originating from the $\pi - \pi^*$ transition with a CT character. We assessed the strong CT character of the $S_0 \rightarrow S_1$ transition by measuring the blue-shift of the S_1 absorption band of meta-HBDI complexed with the betaine zwitterion. Femtosecond pump-probe experiments revealed \sim 100 fs ultrafast relaxation out of the excited S_2 state, followed by population and trapping in the S_1 state for \sim 100 ps. Our experimental observations were rationalized by high-level quantum-chemistry calculations. Three conical intersections were found that interconnect the S_2 , S_1 , and S_0 states, which are relevant to the relaxation dynamics of the meta-chromophore in the gas phase. Although dark, the S_1 state can be populated from the higher-lying bright S_2 state by internal conversion that involves conical intersections. Importantly, this extremely efficient process out-competes and thus suppresses electron detachment from the S_2 electronic resonance. The actual timescale for populating the dark state depends on the potential-energy topography, and the trapping lifetime is determined by energy barriers, along the minimum-energy pathway that leads from the planar S_1 -minimum structure to the highly twisted S_1/S_0 conical intersection. The charge-transfer character of the low-lying dark state provides a direct handle to control its lifetime via the polar environment. This offers a clear design principle for engineering synthetic chromophores with tailored photophysical properties.

Our gas-phase action-absorption and photoelectron spectroscopy study combined with high-level *ab initio* calculations has unequivocally identified a long-lived dark state that acts as an efficient trapping site in the meta-HBDI anion. This discovery and the detailed insight into the charge-transfer character establish a mechanistic framework for understanding photostability, in which dark states act as a general “energy sink”. By dissipating excess electronic energy, these states suppress deleterious electron transfer and photodegradation

following UV excitation. This principle, now revealed in the unperturbed chromophore, may extend to other environments, where similar states could be tuned to enhance photostability or, conversely, to design optical switches. Furthermore, it draws a compelling parallel to the function of dark states in carotenoids, which are critical for photoprotection. By providing direct, gas-phase spectroscopic access to these elusive states, our work establishes a new benchmark for unravelling complex excited-state landscapes, offering a fresh perspective on a cornerstone of biological photochemistry.

Methods

This study employs a unique combination of gas-phase photoabsorption detection, femtosecond time-resolved action spectroscopy, and photoelectron spectroscopy, supported by high-level quantum chemical calculations to interpret the results.

Action-absorption spectroscopy

Action-photoabsorption spectroscopy measurements of meta-HBDI were performed at room temperature at the ion-storage ring ELISA.^{12,13} Methanol - dissolved chromophores were brought into the gas-phase by electrospray ionization, injected into the storage ring and photoexcited by a pulsed nanosecond-laser system (EKSPLA, NT232-50-SH-SFG). The number of neutral fragments after photoexcitation was used as a measure of the absorption cross-section after normalization to the number of photons and stored ions.

Pump-probe time-resolved action-absorption spectroscopy

The relaxation dynamics was investigated by exciting the molecules by fs-laser pulses in the SAPHIRA ion-storage ring at Aarhus University.^{14,15,38} Here the molecules were excited with a 400 nm fs pump-laser pulse into S_2 , and afterwards probed by a 800 nm fs-laser pulse at a variable pump-probe delay. In addition to the short time delay between the two

fs-laser pulses, the molecular-response time by dissociation was recorded by the ion-storage technique. Thus, as pump-probe signal (as a function of the probe-pulse delay) we used the time-resolved yield of neutral photofragments in the storage ring. The advantage of the ion storage ring technique is that it enables the registration of prompt action (fragmentation within the first $10\ \mu\text{s}$ after photoexcitation) as well as delayed action. The counts of prompt neutral fragments after pump and (delayed) probe pulses were created largely by photodetachment rendering a neutral detectable product. The delayed action, on the other hand, appeared when the S_2 state returned to the S_0 ground state by internal conversion, where slow statistical fragmentation and thermionic electron emission occur, typically on the millisecond timescale.

Frequency- and time-resolved photoelectron spectroscopy

Photoelectron spectroscopy measurements were carried out at Durham University.^{16,17} Briefly, electrons were detected and energy analyzed as a function of the photon energy to yield photoelectron spectra.³⁹ In addition, the number of energy-selected photoelectrons were recorded as a function of pump-probe time delay to follow the excited-state relaxation dynamics.

Ab initio calculations

High-level *ab initio* calculations were performed using the multi-state multi-reference perturbation theory XMCQDPT2³³ and complete active space self-consistent field method. The Firefly package⁴⁰ was used for all quantum chemistry calculations. The S_1 excited-state lifetime was computed as functions of ground-state temperature and excitation wavelength within the bright $\text{S}_0 \rightarrow \text{S}_2$ transition using quasi-equilibrium theory for a microcanonical ensemble. The details are described in the Supporting Information.

Acknowledgement

Action-absorption studies were supported by Villum Fonden (Grant No. 17512, L.H.A.). Photoelectron studies were supported by the Engineering and Physical Sciences Research Council (Grant No. EP/Z53545X/1, J.R.R.V.). The theoretical part of this work was supported by the Russian Science Foundation (Grant No. 24-43-00041, A.V.B.). The calculations were carried out using the equipment of the shared research facilities of HPC computing resources at Lomonosov Moscow State University, as well as the local resources (RSC Tornado) provided through the Lomonosov Moscow State University Program of Development.

Supporting Information Available

Supplementary information is available for this article, including computational details and additional computational results.

References

- (1) Polívka, T.; Sundström, V. Ultrafast Dynamics of Carotenoid Excited States From Solution to Natural and Artificial Systems. *Chem. Rev.* **2004**, *104*, 2021–2072.
- (2) Scholes, G. D.; Fleming, G. R.; Olaya-Castro, A.; van Grondelle, R. Lessons from nature about solar light harvesting. *Nat. Chem.* **2011**, *3*, 763–774.
- (3) Berera, R.; van Stokkum, I. H. M.; Gwizdala, M.; Wilson, A.; Kirillovsky, D.; van Grondelle, R. The Photophysics of the Orange Carotenoid Protein, a Light-Powered Molecular Switch. *J. Phys. Chem. B* **2012**, *116*, 2568–2574.
- (4) Frank, H. A.; Bautista, J. A.; Josue, J.; Pendon, Z.; Hiller, R. G.; Sharples, F. P.; Gosz- tola, D.; Wasielewski, M. R. Effect of the Solvent Environment on the Spectroscopic

Properties and Dynamics of the Lowest Excited States of Carotenoids. *J. Phys. Chem. B* **2000**, *104*, 4569–4577.

- (5) Wise, K. J.; Gillespie, N. B.; Stuart, J. A.; Krebs, M. P.; Birge, R. R. Optimization of bacteriorhodopsin for bioelectronic devices. *Trends Biotechnol.* **2002**, *20*, 387 – 394.
- (6) Bhuckory, S.; Kays, J. C.; Dennis, A. M. In Vivo Biosensing Using Resonance Energy Transfer. *Biosensors* **2019**, *9*, 76.
- (7) Yousif, E.; Haddad, R. Photodegradation and photostabilization of polymers, especially polystyrene: review. *SpringerPlus* **2013**, *2*, 398.
- (8) Rocha-Rinza, T.; Christiansen, O.; Rahbek, D. B.; Klærke, B.; Andersen, L. H.; Lincke, K.; Nielsen, M. B. Spectroscopic Implications of the Electron Donor - Acceptor Effect in the Photoactive Yellow Protein Chromophore. *Chem. Eur. J.* **2010**, *16*, 11977–11984.
- (9) Dong, J.; Solntsev, K. M.; Poizat, O.; Tolbert, L. M. The Meta-Green Fluorescent Protein Chromophore. *J. Am. Chem. Soc.* **2007**, *129*, 10084–10085.
- (10) Solntsev, K. M.; Poizat, O.; Dong, J.; Rehault, J.; Lou, Y.; Burda, C.; Tolbert, L. M. Meta and Para Effects in the Ultrafast Excited-State Dynamics of the Green Fluorescent Protein Chromophores. *J. Phys. Chem. B* **2008**, *112*, 2700—2711.
- (11) Bochenkova, A. V.; Klærke, B.; Rahbek, D. B.; Rajput, J.; Toker, Y.; Andersen, L. H. UV Excited-State Photoresponse of Biochromophore Negative Ions. *Angew. Chem. Int. Ed.* **2014**, *53*, 9797–9801.
- (12) Nielsen, S. B.; Lapierre, A.; Andersen, J.; Pedersen, U.; Tomita, S.; Andersen, L. Absorption spectrum of the green fluorescent protein chromophore anion in vacuo. *Phys. Rev. Lett.* **2001**, *87*, 228102.

(13) Andersen, L.; Bluhme, H.; Boyé, S.; Jørgensen, T.; Krogh, H.; Nielsen, I.; Nielsen, S. B.; Svendsen, A. Experimental studies of the photophysics of gas-phase fluorescent protein chromophores. *Phys. Chem. Chem. Phys.* **2004**, *6*, 2617–2627.

(14) Svendsen, A.; Kiefer, H. V.; Pedersen, H. B.; Bochenkova, A. V.; Andersen, L. H. Origin of the intrinsic fluorescence of the green fluorescent protein. *J. Am. Chem. Soc.* **2017**, *139*, 8766–8771.

(15) Kiefer, H. V.; Gruber, E.; Langeland, J.; Kusochek, P. A.; Bochenkova, A. V.; Andersen, L. H. Intrinsic photoisomerization dynamics of protonated Schiff-base retinal. *Nat. Commun.* **2019**, *10*, 1210.

(16) West, C. W.; Bull, J. N.; Antonkov, E.; Verlet, J. R. R. Anion Resonances of para-Benzoquinone Probed by Frequency-Resolved Photoelectron Imaging. *J. Phys. Chem. A* **2014**, *118*, 11346–11354.

(17) Anstöter, C. S.; Bull, J. N.; Verlet, J. R. Ultrafast dynamics of temporary anions probed through the prism of photodetachment. *Int. Rev. Phys. Chem.* **2016**, *35*, 509–538.

(18) Bochenkova, A. V. Multiconfigurational Methods Including XMCQDPT2 Theory for Excited States of Light-Sensitive Biosystems. In *Comprehensive Computational Chemistry (First Edition)*; Yáñez, M., Boyd, R. J., Eds.; Elsevier: Oxford, 2024; pp 141–157.

(19) Bochenkova, A. V.; Andersen, L. H. Ultrafast dual photoresponse of isolated biological chromophores: link to the photoinduced mode-specific non-adiabatic dynamics in proteins. *Faraday Discuss.* **2013**, *163*, 297–319.

(20) Bochenkova, A. V.; Mooney, C. R. S.; Parkes, M. A.; Woodhouse, J. L.; Zhang, L.; Lewin, R.; Ward, J. M.; Hailes, H. C.; Andersen, L. H.; Fielding, H. H. Mechanism of resonant electron emission from the deprotonated GFP chromophore and its biomimetics. *Chem. Sci.* **2017**, *8*, 3154–3163.

(21) Tsien, R. Y. The Green Fluorescent Protein. *Annu. Rev. Biochem.* **1998**, *67*, 509–544.

(22) Andersen, L. H.; Rasmussen, A. P.; Pedersen, H. B.; Beletsan, O. B.; Bochenkova, A. V. High-Resolution Spectroscopy and Selective Photoresponse of Cryogenically Cooled Green Fluorescent Protein Chromophore Anions. *J. Phys. Chem. Lett.* **2023**, *14*, 6395–6401.

(23) Toker, Y.; Rahbek, D.; Klærke, B.; Bochenkova, A.; Andersen, L. Direct and indirect electron emission from the green fluorescent protein chromophore. *Phys. Rev. Lett.* **2012**, *109*, 128101.

(24) Kiefer, H. V.; Pedersen, H. B.; Bochenkova, A. V.; Andersen, L. H. Decoupling Electronic versus Nuclear Photoresponse of Isolated Green Fluorescent Protein Chromophores Using Short Laser Pulses. *Phys. Rev. Lett.* **2016**, *117*, 243004.

(25) Anstöter, C. S.; Mensa-Bonsu, G.; Nag, P.; Ranković, M. c. v.; Kumar T. P., R.; Boichenko, A. N.; Bochenkova, A. V.; Fedor, J.; Verlet, J. R. R. Mode-Specific Vibrational Autodetachment Following Excitation of Electronic Resonances by Electrons and Photons. *Phys. Rev. Lett.* **2020**, *124*, 203401.

(26) Andersen, L. H.; Rasmussen, A. P.; Pedersen, H. B.; Klinkby, N. Valence (S1) and non-valence (dipole-bound) spectroscopy of chromophore models of the photoactive yellow protein probed by cryogenic action spectroscopy. *Phys. Rev. A* **2025**, *112*, 022821.

(27) Stockett, M. H.; Boesen, M.; Houmøller, J.; Nielsen, S. B. Accessing the Intrinsic Nature of Electronic Transitions from Gas-Phase Spectroscopy of Molecular Ion/Zwitterion Complexes. *Angew. Chem. Int. Ed.* **2017**, *56*, 3490–3495.

(28) Shikata, T. Dielectric relaxation behavior of glycine betaine in aqueous solution. *J. Phys. Chem. A* **2002**, *106*, 7664–7670.

(29) Toker, Y.; Langeland, J.; Gruber, E.; Kjær, C.; Nielsen, S. B.; Andersen, L. H.; Borin, V. A.; Schapiro, I. Counterion-controlled spectral tuning of the protonated Schiff-base retinal. *Phys. Rev. A* **2018**, *98*, 043428.

(30) Langeland, J.; Kjær, C.; Andersen, L. H.; Nielsen, S. B. The Effect of an Electric Field on the Spectroscopic Properties of the Isolated Green Fluorescent Protein Chromophore Anion. *ChemPhysChem* **2018**, *19*, 1686–1690.

(31) Mensa-Bonsu, G.; Lietard, A.; Tozer, D. J.; Verlet, J. R. R. Low energy electron impact resonances of anthracene probed by 2D photoelectron imaging of its radical anion. *J. Chem. Phys.* **2020**, *152*, 174303.

(32) Lietard, A.; Verlet, J. R. R.; Slimak, S.; Jordan, K. D. Temporary Anion Resonances of Pyrene: A 2D Photoelectron Imaging and Computational Study. *J. Phys. Chem. A* **2021**, *125*, 7004–7013.

(33) Granovsky, A. A. Extended multi-configuration quasi-degenerate perturbation theory: The new approach to multi-state multi-reference perturbation theory. *J. Chem. Phys.* **2011**, *134*, 214113.

(34) Campbell, E. E. B.; Ulmer, G.; Hertel, I. V. Delayed ionization of C₆₀ and C₇₀. *Phys. Rev. Lett.* **1991**, *67*, 1986–1988.

(35) Horke, D. A.; Li, Q.; Blancafort, L.; Verlet, J. R. R. Ultrafast above-threshold dynamics of the radical anion of a prototypical quinone electron-acceptor. *Nat. Chem.* **2013**, *5*, 711–717.

(36) Bull, J. N.; West, C. W.; Verlet, J. R. R. On the formation of anions: frequency-, angle-, and time-resolved photoelectron imaging of the menadione radical anion. *Chem. Sci.* **2015**, *6*, 1578–1589.

(37) West, C. W.; Bull, J. N.; Hudson, A. S.; Cobb, S. L.; Verlet, J. R. R. Excited State Dynamics of the Isolated Green Fluorescent Protein Chromophore Anion Following UV Excitation. *J. Phys. Chem. B* **2015**, *119*, 3982–3987.

(38) Pedersen, H. B.; Svendsen, A.; Harbo, L. S.; Kiefer, H. V.; Kjeldsen, H.; Lammich, L.; Toker, Y.; Andersen, L. H. Characterization of a new electrostatic storage ring for photofragmentation experiments. *Rev. Sci. Instrum.* **2015**, *86*, 063107.

(39) Lecointre, J.; Roberts, G. M.; Horke, D. A.; Verlet, J. R. R. Ultrafast Relaxation Dynamics Observed Through Time-Resolved Photoelectron Angular Distributions. *J. Phys. Chem. A* **2010**, *114*, 11216–11224.

(40) Granovsky, A. A. Firefly version 8. <http://classic.chem.msu.su>, Accessed on December 09, 2025.

TOC Graphic

